Simultaneous synthesis and amine-functionalization of single-phase BaYF5:Yb/Er nanoprobe for dual-modal in vivo upconversion fluorescence and long-lasting X-ray computed tomography...

ARTICLE *in* NANOSCALE · MAY 2013

Impact Factor: 7.39 · DOI: 10.1039/c3nr00999h · Source: PubMed

Nanoscale

RSC Publishing

PAPER

View Article Online
View Journal | View Issue

Cite this: *Nanoscale*, 2013, **5**, 6023

Simultaneous synthesis and amine-functionalization of single-phase $BaYF_5$:Yb/Er nanoprobe for dual-modal *in vivo* upconversion fluorescence and long-lasting X-ray computed tomography imaging

Hongrong Liu,[a] Wei Lu,[b] Haibo Wang,[c] Ling Rao,[c] Zhigao Yi,[c] Songjun Zeng*[ab] and Jianhua Hao*[b]

In this work, we developed a novel and biocompatible dual-modal nanoprobe based on single-phase amine-functionalized $BaYF_5$:Yb/Er nanoparticles (NPs) for upconversion (UC) fluorescence and *in vivo* computed X-ray tomography (CT) bioimaging for the first time. High-quality water-soluble amine-functionalized $BaYF_5$:Yb/Er NPs with an average size of 24 nm were synthesized by a facile environmentally friendly hydrothermal method for simultaneous synthesis and surface functionalization. Structure investigation based on the Rietveld refinement method revealed that the as-synthesized $BaYF_5$:Yb/Er NPs present a cubic phase structure, which differs from the previously reported tetragonal structure. Under 980 nm excitation, high-contrast green and red UC emissions were observed from HeLa cells incubated with these amine-functionalized NPs. The UC spectra measured from the NPs incubated with HeLa cells presented only green and red UC emissions without any autofluorescence, further revealing that these NPs are ideal candidates for fluorescent bioimaging. In addition, the cell cytotoxicity test showed low cell toxicity of these NPs. These amine-functionalized NPs were also successfully used as CT agents for *in vivo* CT imaging because of the efficient X-ray absorption efficiency of Ba and doped Yb ions. A prolonged (2 h) signal enhancement of the spleen in a mouse was observed in CT imaging, which can improve the detection of splenic diseases. More importantly, the simultaneous X-ray and UC *in vivo* bioimaging was demonstrated in a nude mouse for the first time, indicating the as-prepared UCNPs can be successfully used as dual-modal bioprobes. These results demonstrate that $BaYF_5$:Yb/Er NPs are ideal nanoprobes for dual-modal fluorescent/CT bioimaging with low cytotoxicity, non-autofluorescence, and enhanced detection of the spleen.

Received 26th February 2013
Accepted 25th April 2013

DOI: 10.1039/c3nr00999h

www.rsc.org/nanoscale

1 Introduction

Optical bioimaging is widely used in biomedical studies because it can visualize and understand the function of specific molecules and tissues.[1–3] The optical properties of nanoprobes are crucial to their applications in bioimaging. In the past decades, various fluorescent probes such as organic dyes, fluorescent proteins, and quantum dots have been developed and widely used in the fluorescent bioimaging of cells and tissues.[4–8] Compared with these widely used fluorescent probes, lanthanide-doped upconversion nanoparticles (UCNPs) have emerged as new alternative ideal fluorescent probes for optical bioimaging because of their novel upconversion (UC) property of converting long wavelength excitation to short wavelength emission *via* a two-photon or multi-photon process.[9–25] Using UCNPs as fluorescent probes not only improves the detection sensitivity and signal-to-noise ratio for bioimaging because of the absence of autofluorescence but also increases the penetration depth because of the excitation wavelength located in the "optical transmission window" of biological tissues (750 nm to 1000 nm).[26–30]

Host material is a very important factor in achieving efficient UC luminescence. Among UC host materials, fluorides (MYF, M = Ba, Na, or K) are considered as promising host materials for UC emission under near-infrared laser excitation.[31–33] Bulk $BaYF_5$-doped Er can present approximately eight times brighter UC emission than Er-doped LaF_3.[34] Moreover, glass ceramic containing Er-doped $BaYF_5$ nanocrystals has 13 times brighter UC emission than glass ceramic containing Er-doped LaF_3 nanocrystals.[35] These reports suggest that $BaYF_5$ is

[a]*College of Physics and Information Science and Key Laboratory of Low-dimensional Quantum Structures and Quantum Control of the Ministry of Education, Hunan Normal University, Changsha, Hunan, China. E-mail: songjunz@hunnu.edu.cn*

[b]*Department of Applied Physics and Materials Research Center, The Hong Kong Polytechnic University, Hong Kong. E-mail: apjhhao@polyu.edu.hk*

[c]*Faculty of Materials, Optoelectronics and Physics, Key Laboratory of Low-dimensional Materials and Application Technology (Ministry of Education), Xiangtan University, Xiangtan 411105, People's Republic of China*

a promising host for UC emission. However, only limited reports were focused on nanoscale $BaYF_5$. Recently, Yi *et al.*[36] synthesized lanthanide-doped $BaYF_5$ nanocrystals by co-decomposition in organic solvents under high temperature and inert gas protection. Capobianco *et al.*[37] conducted a UC study on Yb/Tm co-doped $BaYF_5$ NPs synthesized by thermal decomposition. Unfortunately, these hydrophobic $BaYF_5$ NPs need further surface modification for their application in optical bioimaging. Qiu *et al.*[38] reported a controlled synthesis of lanthanide-doped $BaYF_5$ UC nanocrystals by a hydrothermal method using ethylenediaminetetraacetic acid as chelating agent. Despite the promising UC property and preliminary studies on lanthanide-doped $BaYF_5$ UCNPs, reports on the application of these NPs in optical bioimaging are still lacking.

On the other hand, CT is a widely used imaging procedure in diagnostic medicine. Small iodinated molecules are commonly used CT contrast agents because they can effectively absorb X-rays. However, these CT contrast agents suffer from intrinsic drawbacks, including short circulation lifetime and potential renal toxicity.[39,40] Thus, developing new nanoparticulate CT contrast agents with long circulation times and low toxicity is important. Aside from their excellent UC property, $BaYF_5$:Yb/Er UCNPs selected in the present study can act as potential CT contrast agents because of the large K-edge values ($Ba_{K\text{-}edge}$: 37.4 keV, $Yb_{K\text{-}edge}$: 61 keV)[26,40,41] and high X-ray mass absorption coefficients (60 keV, Ba: 8.51 $cm^2\ g^{-1}$, Yb: 3.15 $cm^2\ g^{-1}$; at 80 keV, Ba: 3.96 $cm^2\ g^{-1}$, Yb: 6.91 $cm^2\ g^{-1}$)[42] of Ba and doped Yb. Therefore, the excellent UC emission, together with the large X-ray absorption property, make lanthanide-doped $BaYF_5$ host materials ideal nanoprobes for dual-modal UC fluorescent and CT bioimaging in biomedical applications. These properties can also synergistically combine the advantages of fluorescence and CT imaging while avoiding their individual disadvantages. However, to the best of our knowledge, dual-modal UC fluorescence/CT nanoprobe based on lanthanide-doped $BaYF_5$ host has not yet been exploited.

In this paper, amine-functionalized $BaYF_5$:Yb/Er NPs for UC fluorescent and *in vivo* CT imaging were developed for the first time by a simple hydrothermal method using polyethylenimine (PEI) as surface ligand. The structure and UC property of these NPs were studied. Moreover, the effectiveness of these NPs for optical bioimaging was demonstrated in HeLa cells. Their toxicity was also evaluated in HeLa cells. As shown in *in vivo* CT imaging, these NPs can also be used for CT agents with a long circulation time.

2 Experimental

2.1 Chemicals and materials

Branched PEI (25 kDa) was purchased from Sigma-Aldrich. $Ln(NO_3)_3 \cdot 6H_2O$ (Ln = Y, Yb, Er) was purchased from Sigma-Aldrich. Ethylene glycol (EG), $BaCl_2$ (99.99%), and NH_4F (99.99%) were purchased from Sinopharm Chemical Reagent Co., China.

2.2 Simultaneous synthesis and functionalization of PEI-modified $BaYF_5$:Yb/Er NPs

A modified one-step hydrothermal method[43] was used to synthesize amine-functionalized $BaGdF_5$:Yb/Er UCNPs. In a typical synthesis, 1.5 g PEI was added into 20 mL EG under vigorous stirring. Then, 1 mmol of $Y(NO_3)_3$ (0.5 M), $Yb(NO_3)_3$ (0.5 M), and $Er(NO_3)_3$ (0.1 M) with a molar ratio of 78 : 20 : 2 was added, followed by the addition of 1 mmol $BaCl_2$ to above solution. After 30 min of stirring, 5.0 mmol NH_4F and 10 mL EG were added to the above mixture. After another 30 min of stirring, the above mixture was transferred into a 50 mL stainless Teflon-lined autoclave and stored at 190 °C for 24 h. After the reaction, the system was naturally cooled down to room temperature. The prepared samples were separated by centrifugation, washed several times with ethanol and deionized water to remove other residual solvents, and then dried in a vacuum at 60 °C for 24 h.

2.3 Characterization

The powder X-ray diffraction (XRD) pattern of the as-prepared $BaYF_5$:Yb/Er NPs was detected using a Bruker D8 advance X-ray diffractometer at 40 kV and 200 mA with Cu-Ka radiation (λ = 1.5406 Å). The 2θ ranged from 10° to 75° with a scanning rate of 0.02° per second. The size and morphology of the as-prepared NPs were characterized using a transmission electron microscope (TEM, JEOL-2100F) equipped with an energy-dispersive X-ray spectrometer (EDS). Fourier transform infrared spectrum (FTIR) was recorded by a Magna 760 spectrometer E. S. P. (Nicolet). UC luminescence spectrum was detected by a FLS920P Edinburgh Analytical Instrument apparatus equipped with a 980 nm continuous-wave laser diode with maximum power of 2 W. Digital photographs of the amine-functionalized $BaYF_5$:Yb/Er water solution (1 wt%) were taken using a Canon digital camera.

2.4 Cell culture and *in vitro* optical bioimaging

HeLa cells obtained from the American type Culture Collection (#CCL-185, ATCC, Manassas, VA, USA) were grown in Dulbecco's Modified Eagle's Medium (DMEM) supplemented with 10% fetal bovine serum and 1% penicillin and streptomycin at 37 °C and 5% CO_2. To validate the feasibility of optical bioimaging based on the amine-functionalized $BaYF_5$:Yb/Er UCNPs, HeLa cells incubated with the amine-functionalized $BaYF_5$:Yb/Er UCNPs (100 μg mL^{-1}) were tested by a commercial confocal laser scanning microscope (Leica TCS SP5) under 980 nm excitation. Two typical emission channels were recorded at the green (500 nm to 600 nm) and red (600 nm to 700 nm) spectral regions.

2.5 Cytotoxicity assay

The *in vitro* viability of HeLa cells was measured by the 3-(4,5-dimethylthiazol-2-yl)-2,5-diphenyl-tetrazolium bromide (MTT) proliferation assay method. HeLa cells were seeded into a 96-well microplate (6000 cells per well) and then pre-incubated at 37 °C under 5% CO_2 for 3 h. Then, the cell culture medium in

each well was replaced with DMEM solution containing different concentrations of amine-functionalized $BaYF_5$:Yb/Er UCNPs (100, 200, 500, and 1000 μg mL^{-1}). These HeLa cells were incubated at 37 °C for another 20 h under 5% CO_2. Subsequently, each cell was added with 10 μL MTT labeling solution and then incubated further for 4 h at 37 °C. The absorbance band at 570 nm was measured by Multiskan EX (Thermo Electron Corporation).

2.6 *In vivo* UC/X-ray dual-modal imaging

To demonstrate the *in vivo* UC/X-ray dual-modal imaging, a nude mouse was first anesthetized by intraperitoneal injection of 10 wt% chloral hydrate solution. Then 100 μL of the amine-functionalized $BaYF_4$ UCNPs aqueous solution with concentration of 3 mg mL^{-1} was subcutaneously injected into the nude mouse. After injection, *in vivo* dual-modal imaging was performed by a multi-modal *in vivo* imaging system equipped with an external 980 nm laser diode (adjustable power of 0–30 W) as the excitation source and X-ray imaging functionality (Carestream *In-Vivo* FX PRO). The UC images were captured between 515 and 555 nm using band pass filter (535/20 nm) with exposure time of 20 s. The X-ray images were recorded under the operating voltage of 35 kVp. All animal procedures were in accordance with institutional animal use and care regulations.

2.7 *In vivo* CT imaging

For *in vivo* CT imaging, a mouse was first anesthetized by intraperitoneal injection of 10 wt% chloral hydrate solution. Physiological saline solutions (200 μL) containing the amine-functionalized $BaYF_5$:Yb/Er UCNPs (0.05 M) were then intravenously injected into the mouse *via* the caudal vein. After injection of UCNPs, CT images were acquired at various times (5, 30, 60, and 120 min) using a ZKKS-MCT-Sharp micro-CT (Chinese Academy of Sciences and Guangzhou Kaisheng Medical Technology Co., Ltd.). The parameters of CT images were as follows: thickness, 0.14 mm; pitch, 0.07; 60 kVp, 0.5 mA; large field of view; gantry rotation time, 0.5 s; speed, 5 mm s^{-1}.

3 Results and discussion

3.1 Synthesis and structure characterization

The simultaneously synthesized and functionalized hydrothermal method using PEI as capping ligand were developed to synthesize amine-functionalized $BaYF_5$:Yb/Er (doped with 20% Yb/2% Er) UCNPs. The structure and phase composition of the as-prepared UCNPs were detected by XRD. Eight characteristic diffraction peaks located at 26.12°, 30.34°, 43.56°, 51.62°, 54.159°, 63.479°, 69.96°, and 72.098° were detected in the XRD pattern (Fig. 1) of the as-prepared $BaYF_5$:Yb/Er UCNPs (blue line). Compared with the standard tetragonal $BaYF_5$ (JCPDS 46-0039) and cubic $BaCeF_5$ (JCPDS 43-0394), all diffraction peaks matched well with the latter. This finding suggests that the as-prepared $BaYF_5$:Yb/Er UCNPs possess a cubic structure[44] rather than a tetragonal structure. To further verify this result, we carried out Rietveld refinement on the experimental data using Jade 6.5 software by the least-squares method. As demonstrated

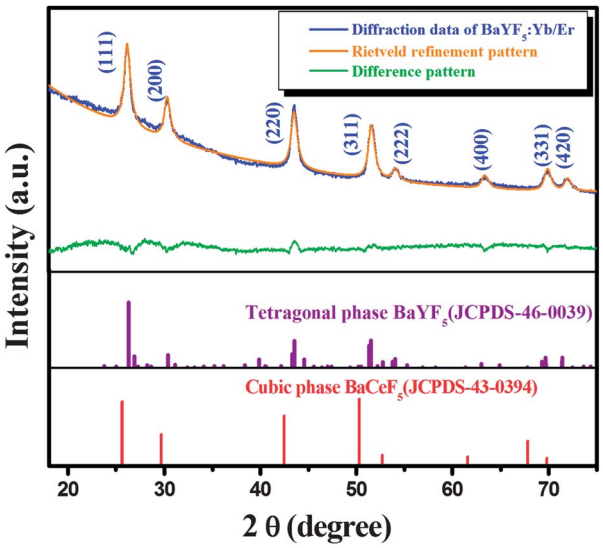

Fig. 1 XRD patterns of the amine-functionalized $BaYF_5$:Yb/Er UCNPs. The blue line is experimental diffraction data, the yellow line is Rietveld refinement pattern, the green curve is the difference between the experimental and calculated intensities in the same scale, the purple line indicates the standard tetragonal $BaYF_5$ (JCPDS: 46-0039), and the red line is the standard cubic $BaCeF_5$ (JCPDS: 43-0394).

in Fig. 1, the Rietveld refinement pattern (yellow line) was well consistent with the experimental diffraction pattern (blue line) with acceptable reliability factors $R = 3.52\%$. This result further verifies that the as-synthesized UCNPs possess a cubic-phase structure. The lattice constant was calculated to be 5.852 Å. Moreover, no other impurity diffraction peaks were observed, indicating that all of the doping ions were successfully incorporated into the host materials. TEM characterizations were performed to reveal the size and morphology of the as-synthesized $BaYF_5$:Yb/Er UCNPs. The typical TEM image in Fig. 2a shows that the as-prepared NPs are highly dispersed. The size-distribution of the as-prepared UCNPs (inset of Fig. 2a) show that the average size is approximately 24 nm ± 2.2 nm. The corresponding selected area electron diffraction pattern (Fig. 2b) proved that the as-prepared UCNPs have a face-centered cubic (FCC) structure, which is consistent with the aforementioned XRD analysis. Fig. 2c shows the typical high-resolution TEM image of a single particle with a measured *d*-spacing of 2.95 Å, which corresponds to the (200) lattice plane of the cubic $BaYF_5$. As demonstrated in EDS analysis (Fig. 2d), the as-prepared UCNPs were mainly composed of Ba, Y, F, and the doped Yb.

3.2 FTIR analysis

PEI grafted on the surface of the NPs can facilitate the cellular uptake by endocytosis because of its positive charge.[45] FTIR analysis of the amine-functionalized UCNPs was performed to reveal the attachment of PEI on the surface of the NPs. As shown in Fig. 3, the weak absorption peaks at 2928 and 2835 cm^{-1} are attributed to the asymmetric and symmetric stretching vibrations of the C–H bond, respectively. The absorption band at

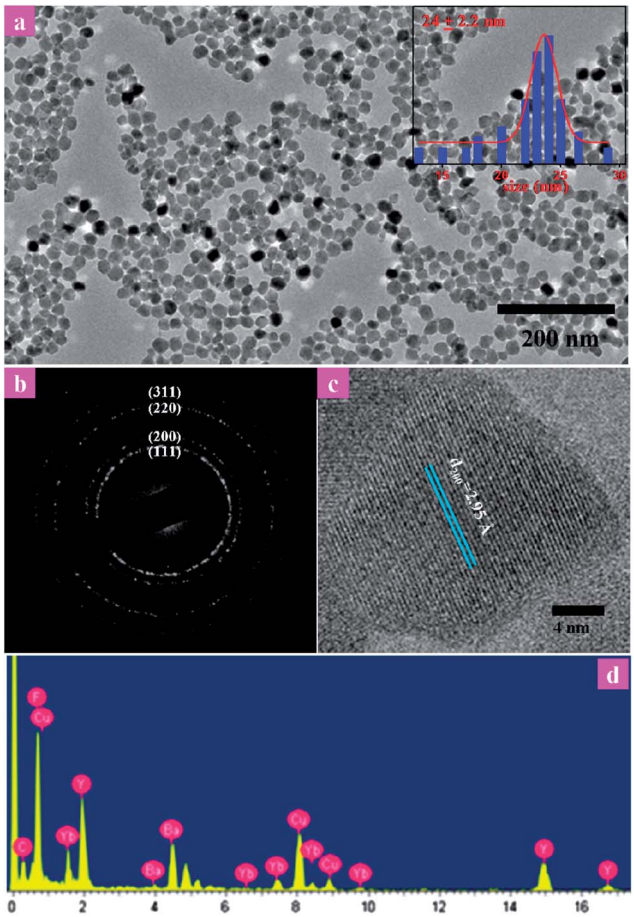

Fig. 2 Typical TEM and EDS results of the amine-functionalized $BaYF_5$:Yb/Er UCNPs: (a) TEM image, (b) corresponding SAED pattern indicating the face center cubic phase structure, (c) HRTEM image of an individual particle, and (d) EDS pattern. The inset of (a) indicates the size distribution of the particle.

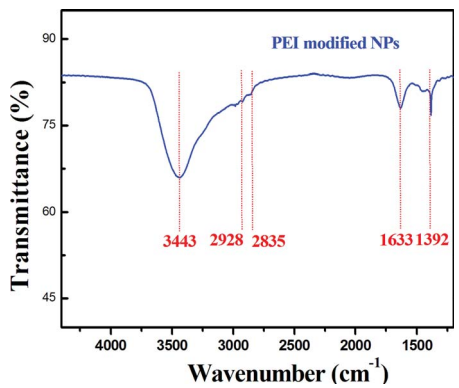

Fig. 3 FTIR spectrum of the amine-functionalized $BaYF_5$:Yb/Er UCNPs.

1392 cm^{-1} is mainly ascribed to the stretching vibrations of the C–N bond. Two strong absorption bands located at 1633 and 3443 cm^{-1} are attributed to the N–H bending mode of amino groups ($-NH_2$)[46] and the stretching vibration of amine groups, respectively, indicating the successful attachment of PEI on the surface of the NPs.

3.3 UC luminescent properties

The UC luminescent properties of the as-prepared $BaYF_5$:Yb/Er UCNPs were detected under 980 nm excitation. Fig. 4a shows the typical UC luminescent spectrum of the amine-functionalized $BaYF_5$:Yb/Er UCNPs. Fig. 4a shows three typical UC emission bands centered at 520/541 (green) and 652 (red) nm, which can be attributed to the electronic transition $^2H_{11/2}/^4S_{3/2} \rightarrow {}^4I_{15/2}$ and $^4F_{9/2} \rightarrow {}^4I_{15/2}$ of Er^{3+} ions based on the energy level diagram (Fig. 4b), respectively. The left inset of Fig. 4a shows a photograph of the 1 wt% water solution of the amine-functionalized $BaYF_5$:Yb/Er UCNPs, indicating that these NPs can emit eye-visible green UC luminescence. To further reveal the UC mechanism, the UC luminescent intensity was detected as a function of the excitation power. In a general UC luminescent process, the UC luminescent intensity (I_{UC}) is proportional to the infrared excitation (I_{IR}) power, which can be described with the following formula:[47]

$$I_{UC} \propto I_{IR}^{n}.$$

Where n is the photon numbers absorbed for per UC emission. The value of n was determined by the slope of the fitted line of the plot log I_{UC} *versus* log I_{IR}.

As shown in the right inset of Fig. 4a, the slopes for the green and red UC emissions of Er^{3+} at 520, 541, and 652 nm are 1.91, 1.79, and 1.65, respectively. These features indicate that both

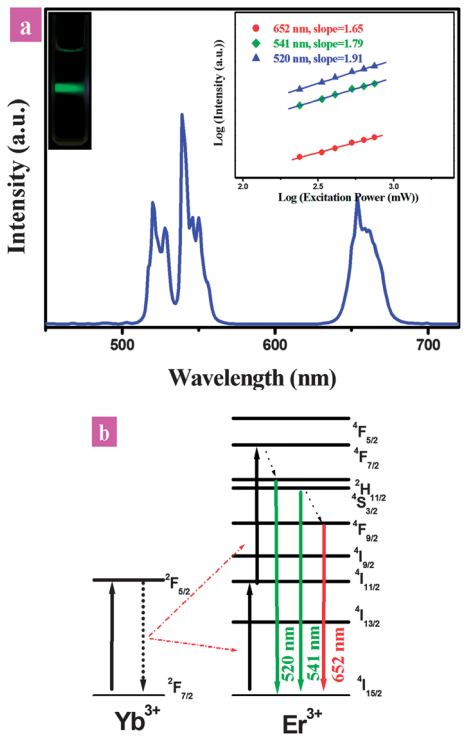

Fig. 4 (a) Upconversion spectrum of the amine-functionalized $BaYF_5$:Yb/Er UCNPs, (b) schematic energy levels of Yb^{3+} and Er^{3+} ions. The left inset of Fig. 3a shows the photograph of the 1 wt% water solution of UCNPs under 980 nm excitation with power density of 5 W cm^{-2}. The right inset of Fig. 3b is the log–log plots of the upconversion luminescence intensity *versus* excitation power.

green and red UC emissions require a two-photon process in the $BaYF_5$ host.

3.4 *In vitro* UC fluorescent bioimaging

To reveal the UC fluorescent bioimaging, HeLa cells incubated with the amine-functionalized $BaYF_5$:Yb/Er UCNPs were imaged by a confocal laser scanning microscope under 980 nm excitation. Two UC signals at 500 nm to 600 nm (green channel) and 600 nm to 700 nm (red channel) were detected. Fig. 5 shows the UC fluorescent bioimaging of HeLa cells treated with these amine-functionalized UCNPs (100 μg mL^{-1}) for 24 h incubation at 37 °C and 5% CO_2. As shown in Fig. 5, the HeLa cells treated with the UCNPs exhibited bright green (Fig. 5b) and red (Fig. 5c) luminescence, indicating that the amine-functionalized UCNPs were successfully internalized into the cells. The insets of Fig. 5b and c show the corresponding UC spectra detected by the confocal laser scanning microscope under bioimaging. Intense 520/541 (green) and 652 (red) UC emissions of Er^{3+} without any autofluorescence were observed, further verifying the successful cellular uptake of these UCNPs. The above results suggest that these amine-functionalized $BaYF_5$:Yb/Er UCNPs can be used as ideal nanoprobes for UC fluorescent bioimaging without autofluorescence.

3.5 Cell cytotoxicity test

To further reveal the biocompatibility of these UCNPs, cell cytotoxicity was measured by the MTT method in HeLa cells. Fig. 6 shows the cell viability of the HeLa cells incubated with different concentrations of the amine-functionalized $BaYF_5$:Yb/Er UCNPs for 24 h at 37 °C and 5% CO_2. As demonstrated in Fig. 6, the viability of the HeLa cells was 98% at 100 μg mL^{-1} UCNP concentration. No significant differences were observed when UCNP concentration was increased to 500 μg mL^{-1}. The cellular viability was estimated to be 83% even when the concentration of UCNPs was further increased to 1000 μg mL^{-1}. These results demonstrate that the amine-functionalized UCNPs (100 μg mL^{-1}) used in bioimaging have low cell toxicity. Therefore, the amine-functionalized UCNPs with low cytotoxicity and excellent UC emission without autofluorescence are promising candidates for optical bioimaging.

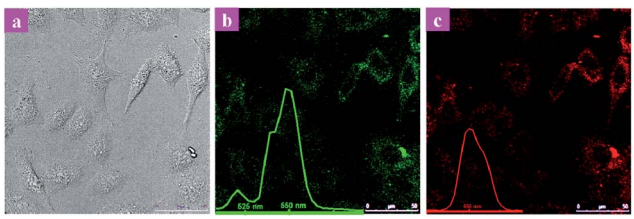

Fig. 5 *In vitro* upconversion fluorescent bioimaging of HeLa cells treated with the amine-functionalized $BaYF_5$:Yb/Er UCNPs under 980 nm excitation: (a) bright field image of HeLa cells, (b) corresponding green upconversion fluorescent image (500 nm to 600 nm), (c) red upconversion fluorescent image (600 nm to 700 nm). The insets of (b) and (c) show the corresponding photoluminescence spectra taken from HeLa cells in the green (500 nm to 600 nm) and red regions (600 nm to 700 nm) under 980 nm excitation, respectively.

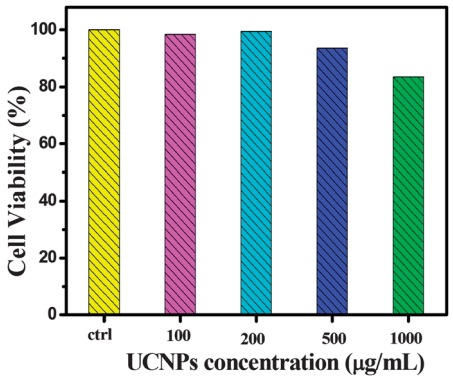

Fig. 6 Cell cytotoxicity of the amine-functionalized $BaYF_5$:Yb/Er UCNPs in HeLa cells treated with different concentrations of these UCNPs at 37 °C for 24 h under 5% CO_2.

3.6 *In vivo* UC fluorescent bioimaging

Owing to the low cell cytotoxicity, we further demonstrated the *in vivo* UC fluorescent bioimaging in a nude mouse. Fig. 7 presents the *in vivo* whole-body images of a nude mouse with and without subcutaneous injection of the amine-functionalized UCNPs. The UC images of the mouse were collected by Carestream *In-Vivo* FX PRO multi-modal *in vivo* imaging system equipped with an external 980 nm laser as the excitation source. As demonstrated in Fig. 7b, a significant UC signal was observed after subcutaneous injection, whereas no UC signal was observed without administration of UCNPs (Fig. 7a). The high contrast *in vivo* imaging between the background and UC imaging area indicates that the as-prepared NPs have potential applications in *in vivo* imaging of animals.

3.7 *In vivo* CT imaging of a mouse

Aside from the excellent UC and optical bioimaging properties demonstrated above, the amine-functionalized $BaGdF_5$:Yb/Er

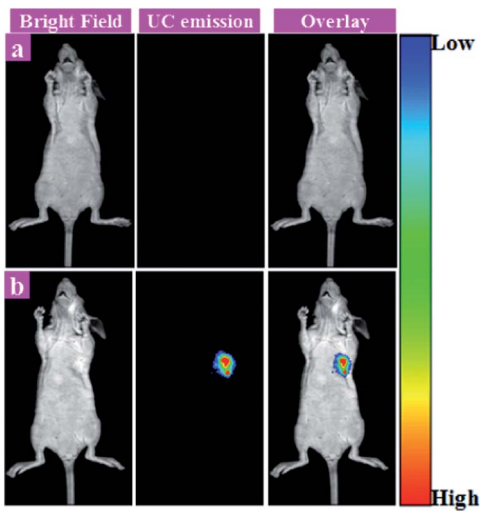

Fig. 7 *In vivo* upconversion fluorescent bioimaging of a nude mouse: (a) without subcutaneous injection of UCNPs, (b) with subcutaneous injection of UCNPs.

UCNPs can also be used as CT contrast agents because of the high X-ray absorption coefficient of Ba and doped Yb in the host matrix. To evaluate the feasibility of these UCNPs as CT contrast agents, a physiological saline solution containing these UCNPs was intravenously injected into a mouse *via* the caudal vein. After injection, CT images of the mouse were acquired at different time intervals. Fig. 8 shows the typical *in vivo* X-ray CT imaging of a mouse at different time periods after injection of 200 μL physiological saline solution containing the amine-functionalized $BaYF_5$:Yb/Er UCNPs (0.05 M): (a) maximum intensity projection (MIP), (b) the corresponding 3D volume-rendered (VR) CT images, and (c) lateral view of 3D VR CT images. As demonstrated in the pre-injection image, no signals of the soft tissues were observed *via* X-ray CT imaging. After administration for 5 min, an obvious enhancement of the signal of the spleen was detected. As the time was prolonged from 30 min to 120 min, a significant signal enhancement of the spleen was still observed. These features indicate that these amine-functionalized $BaYF_5$:Yb/Er UCNPs can be considered as ideal CT imaging probes for the detection of splenic diseases. The long-lasting signal enhancement of the spleen may improve the detection of diseases. More importantly, the large different absorption abilities of Ba and doped Yb under different operating voltages (at 60 keV, Ba: 8.51 $cm^2\ g^{-1}$, Yb: 3.15 $cm^2\ g^{-1}$; at 80 keV, Ba: 3.96 $cm^2\ g^{-1}$, Yb: 6.91 $cm^2\ g^{-1}$)[42] make these amine-functionalized $BaYF_5$:Yb/Er UCNPs suitable for the diagnostic imaging of various patients.

3.8 Simultaneous X-ray and UC bioimaging

To further demonstrate the dual-modal X-ray and UC bioimaging in a same system. Simultaneous X-ray and UC bioimaging of a nude mouse was tested by a multi-modal Carestream *In-Vivo* FX PRO *in vivo* imaging system equipped with an external 980 nm laser as the excitation source and X-ray imaging facility. The whole body dual-modal X-ray and UC imaging of UCNPs in a nude mouse is presented in Fig. 9. As demonstrated in Fig. 9b, the obvious X-ray absorption contrast

Fig. 8 *In vivo* X-ray CT imaging of a mouse before and after intravenous injection of the amine-functionalized $BaYF_5$:Yb/Er UCNPs at various times: (a) maximum intensity projections, (b) the corresponding 3D volume-rendered (VR) *in vivo* CT images of the mouse, and (c) lateral view of 3D VR CT images.

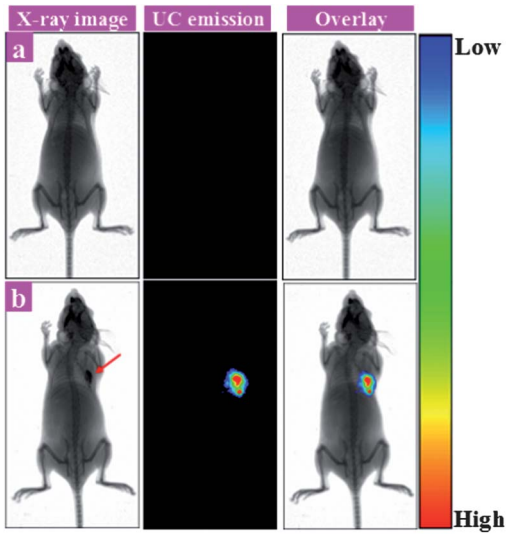

Fig. 9 *In vivo* dual-modal X-ray and UC bioimaging of a nude mouse: (a) without subcutaneous injection of UCNPs, (b) with subcutaneous injection of UCNPs. The left panel: X-ray imaging, the middle panel: UC imaging, the right panel: the overlay images.

(indicated by red arrow) can be observed after subcutaneous injection of UCNPs, whereas no X-ray signal was observed without administration of UCNPs (Fig. 9a). More importantly, the high contrast UC signal was also obtained at the same region (the middle panel of Fig. 9b). As shown in the right panel of Fig. 9b, the UC and the X-ray signals were matched very well, indicating the as-prepared UCNPs can be successfully used as dual-modal nanoprobes.

4 Conclusions

New amine-functionalized $BaYF_5$:Yb/Er nanoprobes for dual-modality UC fluorescent and *in vivo* CT bioimaging was developed by a simultaneous synthesis and functionalization hydrothermal method using PEI as capping ligand. The XRD and TEM results revealed that the as-prepared $BaYF_5$:Yb/Er UCNPs present an FCC cubic structure with an average size of 24 nm and high monodispersity. The amine-functionalized $BaYF_5$:Yb/Er UCNPs presented efficient green and red UC luminescence and were successfully used as probes for the UC fluorescent bioimaging of HeLa cells. Moreover, the spectra of HeLa cells treated with these UCNPs under 980 nm excitation matched well with the UC emission of Er^{3+}, indicating that these UCNPs are ideal nanoprobes for optical bioimaging without autofluorescence. In addition, the cell toxicity test showed that these UCNPs have low cytotoxicity even when the concentration was increased to 1000 μg mL^{-1}. In addition, these UCNPs can also be used as new CT imaging agents. After intravenous injection of these UCNPs, a long-lasting signal enhancement of the spleen was clearly observed for 2 h, which can improve the detection of splenic diseases. More interestingly, two different X-ray contrast elements such as Ba and doped Yb contained in these single phase $BaYF_5$:Yb/Er UCNP host materials make these UCNPs suitable for various clinical

applications at different operating voltages. Overall, the excellent UC fluorescent bioimaging together with the *in vivo* CT imaging make the amine-functionalized $BaYF_5$:Yb/Er UCNPs ideal dual-modal nanoprobes for biomedical applications.

Acknowledgements

This work was supported by the National Natural Science Foundation of China (no. 51102202, 31070663, and 91230116), specialized research Fund for the Doctoral Program of Higher Education of China (no. 20114301120006) and Hunan Provincial Natural Science Foundation of China (no. 12JJ4056 and 13JJ1017), the Scientific Foundation of Ministry of Education and Education Department of Hunan Province, China (212119 and 11A124).

Notes and references

1 J. Zhou, Z. Liu and F. Y. Li, *Chem. Soc. Rev.*, 2012, **41**, 1323.
2 J. H. Lee, Y. M. Huh, Y. Jun, J. Seo, J. Jang, H. T. Song, S. J. Kim, E. J. Cho, H. G. Yoon, J. S. Suh and J. W. Cheon, *Nat. Med.*, 2007, **13**, 95.
3 P. Sharma, S. Brown, G. Walter, S. Santra and B. Moudgil, *Adv. Colloid Interface Sci.*, 2006, **123**, 471.
4 J. E. H. Buston, J. R. Young and H. L. Anderson, *Chem. Commun.*, 2000, 905.
5 R. Heim, A. B. Cubitt and R. Y. Tsien, *Nature*, 1995, **373**, 663.
6 B. C. Lagerholm, M. M. Wang, L. A. Ernst, D. H. Ly, H. J. Liu, M. P. Bruchez and A. S. Waggoner, *Nano Lett.*, 2004, **4**, 2019.
7 T. Jamieson, R. Bakhshi, D. Petrova, R. Pocock, M. Imani and A. M. Seifalian, *Biomaterials*, 2007, **28**, 4717.
8 X. H. Gao, Y. Y. Cui, R. M. Levenson, L. W. K. Chung and S. M. Nie, *Nat. Biotechnol.*, 2004, **22**, 969.
9 F. Vetrone, R. Naccache, A. Juarranz de la Fuente, F. Sanz-Rodríguez, A. Blazquez-Castro, E. M. Rodriguez, D. Jaque, J. G. Solé and J. A. Capobianco, *Nanoscale*, 2010, **2**, 495.
10 J. C. Zhou, Z. L. Yang, W. Dong, R. J. Tang, L. D. Sun and C. H. Yan, *Biomaterials*, 2011, **32**, 9059.
11 M. Nyk, R. Kumar, T. Y. Ohulchanskyy, E. J. Bergey and P. N. Prasad, *Nano Lett.*, 2008, **8**, 3834.
12 D. K. Chatteriee, A. J. Rufalhah and Y. Zhang, *Biomaterials*, 2008, **29**, 937.
13 J. Zhou, Y. Sun, X. X. Du, L. Q. Xiong, H. Hu and F. Y. Li, *Biomaterials*, 2010, **31**, 3287.
14 M. Wang, C. C. Mi, W. X. Wang, C. H. Liu, Y. F. Wu, Z. R. Xu, C. B. Mao and S. K. Xu, *ACS Nano*, 2009, **3**, 1580.
15 M. Haase and H. Schäfer, *Angew. Chem., Int. Ed.*, 2011, **50**, 5808.
16 C. Wang, L. Cheng and Z. Liu, *Biomaterials*, 2011, **32**, 1110.
17 J. Zhou, M. Yu, Y. Sun, X. Zhang, X. Zhu, Z. Wu, D. M. Wu and F. Y. Li, *Biomaterials*, 2011, **32**, 1148.
18 H. Xu, L. Cheng, C. Wang, X. Ma, Y. Li and Z. Liu, *Biomaterials*, 2011, **32**, 9364.
19 R. Kumar, M. Nyk, T. Y. Ohulchanskyy, C. A. Flask and P. N. Prasad, *Adv. Funct. Mater.*, 2009, **19**, 853.
20 F. Wang and X. G. Liu, *Chem. Soc. Rev.*, 2009, **38**, 976.
21 F. Wang, D. Banerjee, Y. S. Liu, X. Y. Chen and X. G. Liu, *Analyst*, 2010, **135**, 1839.
22 Z. Q. Li, Y. Zhang and S. Jiang, *Adv. Mater.*, 2008, **20**, 4765.
23 S. J. Zeng, M. K. Tsang, C. F. Chan, K. L. Wong, B. Fei and J. H. Hao, *Nanoscale*, 2012, **4**, 5118.
24 Z. L. Wang, J. H. Hao, H. L. W. Chan, W. T. Wong and K. L. Wong, *Small*, 2012, **8**, 1863.
25 Z. L. Wang, J. H. Hao, H. L. W. Chan, G. L. Law, W. T. Wong, K. L. Wong, M. B. Murphy, T. Su, Z. H. Zhang and S. Q. Zeng, *Nanoscale*, 2011, **3**, 2175.
26 S. J. Zeng, M. K. Tsang, C. F. Chan, K. L. Wong and J. H. Hao, *Biomaterials*, 2012, **33**, 9232.
27 J. Wang, F. Wang, C. Wang, Z. Liu and X. G. Liu, *Angew. Chem., Int. Ed.*, 2011, **50**, 10369.
28 S. W. Wu, G. Han, D. J. Milliron, S. Aloni, V. Altoe, D. V. Talapin, B. E. Cohen and P. J. Schuck, *Proc. Natl. Acad. Sci. U. S. A.*, 2009, **106**, 10917.
29 L. Cheng, K. Yang, Y. G. Li, J. H. Chen, C. Wang, M. W. Shao, S. T. Lee and Z. Liu, *Angew. Chem., Int. Ed.*, 2011, **50**, 7385.
30 Q. Liu, Y. Sun, T. S. Yang, W. Feng, C. G. Li and F. Y. Li, *J. Am. Chem. Soc.*, 2011, **133**, 17122.
31 Z. Q. Li and Y. Zhang, *Angew. Chem., Int. Ed.*, 2006, **45**, 7732.
32 K. W. Kramer, D. Biner, G. Frei, H. U. Gudel, M. P. Hehlen and S. R. Luthi, *Chem. Mater.*, 2004, **16**, 1244.
33 C. M. Zhang, P. A. Ma, C. X. Li, G. G. Li, S. S. Huang, D. M. Yang, M. M. Shang, X. J. Kang and J. Lin, *J. Mater. Chem.*, 2011, **21**, 717.
34 H. J. Guggenheim and L. F. Johnson, *Appl. Phys. Lett.*, 1969, **15**, 51.
35 F. Liu, Y. S. Wang, D. Q. Chen, Y. Yu, E. Ma, L. H. Zhou and P. Huang, *Mater. Lett.*, 2007, **61**, 5022.
36 G. S. Yi, W. B. Lee and G. M. Chow, *J. Nanosci. Nanotechnol.*, 2007, **7**, 2790.
37 F. Vetrone, V. Mahalingam and A. Capobianco, *Chem. Mater.*, 2009, **21**, 1847.
38 H. L. Qiu, G. Y. Chen, L. Sun, S. W. Hao, G. Han and C. H. Yang, *J. Mater. Chem.*, 2011, **21**, 17202.
39 C. Haller and I. Hizoh, *Invest. Radiol.*, 2004, **39**, 149.
40 Y. L. Liu, K. L. Ai, J. H. Liu, Q. H. Yuan, Y. Y. He and L. H. Lu, *Angew. Chem., Int. Ed.*, 2012, **51**, 1437.
41 S. B. Yu and A. D. Watson, *Chem. Rev.*, 1999, **99**, 2353.
42 http://physics.nist.gov/PhysRefData/XrayMassCoef/.
43 F. Wang and X. G. Liu, *J. Am. Chem. Soc.*, 2008, **130**, 5642.
44 Y. J. Huang, H. P. You, G. Jia, Y. H. Song, Y. H. Zheng, M. Yang, K. Liu and N. Guo, *J. Phys. Chem. C*, 2010, **114**, 18051.
45 J. F. Jin, Y. J. Gu, C. W. Y. Man, J. P. Cheng, Z. H. Xu, Y. Zhang, H. S. Wang, V. H. Y. Lee, S. H. Cheng and W. T. Wong, *ACS Nano*, 2011, **5**, 7838.
46 D. T. Tu, Y. S. Liu, R. F. Li, H. M. Zhu, J. C. Chen, Z. Chen, M. D. Huang and X. Y. Chen, *J. Am. Chem. Soc.*, 2012, **134**, 1323.
47 G. Z. Ren, S. J. Zeng and J. H. Hao, *J. Phys. Chem. C*, 2011, **115**, 20141.